

A Simple Guiding Principle for the Temperature Dependence of the Solubility of Light Gases in Imidazolium-based Ionic Liquids Derived from Molecular Simulations

Daniela Kerl^{1,*}, Majid Namayandeh Jorabchi², Ralf Ludwig^{3,4}, Sebastian Wohlrab⁴, and Dietmar Paschek^{2,†}

¹*FB 4 Produktionstechnik, Universität Bremen, Badgasteiner Str. 1, D-28359 Bremen, Germany*

²*Institut für Chemie, Physikalische und Theoretische Chemie, Universität Rostock, Albert-Einstein-Str. 21, D-18059 Rostock, Germany*

³*Institut für Chemie, Physikalische und Theoretische Chemie, Universität Rostock, Dr.-Lorenz-Weg 1, D-18059 Rostock, Germany*

⁴*Leibniz-Institut für Katalyse an der Universität Rostock, Albert-Einstein-Str. 29a, D-18059 Rostock, Germany*

(Dated: August 24, 2018)

We have determined the temperature dependence of the solvation behavior of a large collection of important light gases in imidazolium-based Ionic Liquids (ILs) with the help of extensive molecular dynamics simulations. The motivation of our study is to unravel common features of the temperature dependent solvation under well controlled conditions, and to provide a guidance for cases, where experimental data from different sources disagree significantly. The solubility of molecular hydrogen, oxygen, nitrogen, methane, krypton, argon, neon and carbon dioxide in the imidazolium based ILs of type 1-*n*-alkyl-3-methylimidazolium bis(trifluoromethylsulfonyl)imide ($[C_n\text{mim}][\text{NTf}_2]$) with varying chain lengths $n=2, 4, 6, 8$ are computed for a temperature range between 300 K and 500 K at 1 bar. By applying Widom's particle insertion technique and Bennet's overlapping distribution method, we are able to determine the temperature dependent solvation free energies for those selected light gases in simulated imidazolium based ILs with high statistical accuracy. Our simulations demonstrate that the magnitude of the solvation free energy of a gas molecule at a chosen reference temperature and its temperature-derivatives are intimately related with respect to one another. We conclude that this "universal" behavior is rooted in a solvation entropy-enthalpy compensation effect, which seems to be a defining feature of the solvation of small molecules in Ionic Liquids. We argue that this feature is based on a hypothesized funnel-like shape of the free energy landscape of a solvated gas molecule. The observations lead to simple analytical relations, determining the temperature dependence of the solubility data based on the absolute solubility at a certain reference temperature, which we call "solvation funnel" model. By comparing our results with available experimental data from many sources, we can show that the "solvation funnel" model is particularly helpful for providing reliable estimates for the solvation behavior of very light gases, such as hydrogen, where conflicting experimental data exist.

INTRODUCTION

Salts with melting points below 100°C are commonly referred to as Ionic liquids (ILs). These liquids have several unique properties [1–4], and are discussed for a wide range of potential applications [5, 6]. For the application of ILs in gas separation processes (e.g. for flue gas decontamination) it is important to have access to accurate solubility data. [7–10]. Even more so, the recently introduced Supported Ionic Liquids Membranes [11–14] are a promising new tool for separating various mixtures of gases. Of particular importance, of course, is the ability to separate of H₂ and CO₂ from gas-streams.

Since now, a wealth of experimental measurements of the infinite dilution properties for a large number of gases in various ILs have been reported [15]. However, the experimental determination of solubilities is particularly difficult for gases with a low molecular weight [1]. As result, for example, the reported solubility data of hydrogen in ILs [16–26] are highly inconsistent.

In addition, also theoretical methods to determine solubilities of gases in imidazolium-based ILs have been reported in literature: Data were determined from

COSMO based methods [27–30], equations of state approaches [31–34], group theory [35], quantitative structure-property relationship (QSPR) and neutral network models [36], as well as, molecular dynamics (MD) and Monte Carlo (MC) simulations [37–53]. We would like to point out that MD and MC simulations have the advantage that they offer the possibility of both, a (semi-)quantitative prediction of the solubility, as well as gaining a fundamental understanding of the molecular mechanism for the solvation process.

For the simulation of imidazolium-based ILs there are different atomic-detailed molecular force fields available [54]. Many of those force-fields are capable of reproducing essentially "static" properties, such as thermodynamic properties and structural features quite well. However, most of them are lacking the ability of describing transport properties, such as diffusion coefficients and viscosities satisfactorily. In this study we used the non-polarizable all-atom forcefield originally introduced by Lopes [55], using the refined parameters of Köddermann et al. [56] to simulate the imidazolium-based ILs of type $[C_n\text{mim}][\text{NTf}_2]$ (see Figure 1). We have shown earlier that a wealth of both, thermodynamical and dynamical

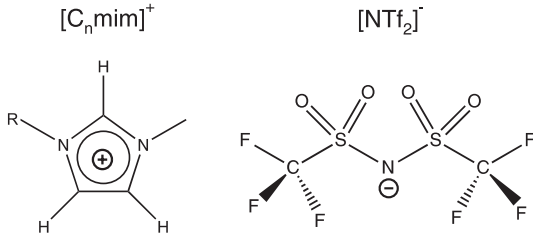


FIG. 1: Schematic representation of the studied ionic liquids 1-n-alkyl-3-methylimidazolium bis(trifluoromethylsulfonyl)imide $[C_n\text{mim}][\text{NTf}_2]$.

properties of the pure IL could be described in excellent agreement with experimental data [40, 56] by using this model. In addition, this modified forcefield was also capable describing the solvation behavior of noble gases [57] and carbon dioxide [58] very satisfactorily. By accurately determining temperature dependent solvation properties, we could demonstrate that the entropy contribution to the solvation free energy plays an important role in the solvation process, not unlike the hydrophobic hydration of small apolar particles in liquid water [59–62]. Moreover, also an entropy-driven “solvophobic interaction” of apolar particles could be observed in ILs [57], indicating that specific solvent-mediated interactions could play an important role in ILs.

Here we focus on the infinite dilution properties of “light gases”, like carbon dioxide, oxygen, nitrogen, methane, argon, neon, and hydrogen in imidazolium based Ionic Liquids. The chosen gases cover a spectrum from very weakly interacting gases, such as hydrogen, to moderately strong interacting molecules, such as carbon dioxide. We apply Widom’s particle insertion technique for calculating temperature dependent solvation free energies and solubilities of these gases in imidazolium-based ionic liquids of the type $[C_n\text{mim}][\text{NTf}_2]$ with varying chain lengths. $n = 2, 4, 6, 8$. In addition, to validate these calculations we also use Bennett’s overlapping distribution method for selected examples. The calculated Henry constants are compared with available experimental data. The temperature behavior of the solubility as well as its dependence of the alkyl-chain lengths in the imidazolium cations is determined and discussed. The motivation of our study is to reveal common “universal” features of the temperature dependent solvation under well controlled conditions, and to provide a reasonable guidance for cases, where experimental data from different sources disagree significantly.

TABLE I: Forcefield parameters describing the studies gaseous solutes. Given are the Lennard-Jones parameter for the solute-solute site-site interactions σ_{ii} , and ε_{ii} , the partial charges q_i , as well as the intramolecular bond-lengths d . Lennard-Jones cross parameters for the solute-solvent interactions were obtained from Lorentz-Berthelot combination rules.

		$\varepsilon_{ii} \cdot k_B^{-1}/\text{K}$	$\sigma_{ii}/\text{\AA}$	$q_i/ e $	$d/\text{\AA}$
H ₂ [64]		35.45	3.46		
Ne [65]		18.6	3.035		
Ar [65]		125.0	3.415		
Kr [65]		169.0	3.675		
CH ₄ [65]		147.4	3.73		
N ₂ [66]	N	36.0	3.31	-0.482	1.10
	COM			+0.964	
O ₂ [67]	O	49.048	3.013	-0.123	1.21
	COM			+0.246	
CO ₂ [68]	C	28.129	2.757	+0.6512	1.149
	O	80.507	3.033	-0.3256	

EXPERIMENTAL SECTION

Molecular Dynamics Simulations

We perform constant pressure (NPT) MD simulations of imidazolium based ILs of the type $[C_n\text{mim}][\text{NTf}_2]$ for different chain lengths $n = 2, 4, 6, 8$ at a pressure of 1 bar, covering a broad temperature range between 300 K and 500 K. All simulated systems are composed of 343 ion pairs, applying the forcefield of Lopes et al. [55] with refined potential parameters according to Köddermann et al. [56]. An additional minor modification from the simulation setup used in previous studies [40, 56] is that *all* bond-lengths were kept fixed. A cubic simulation box was used, and the system size with 343 ion pairs was chosen large enough that thermodynamical properties do not depend on the system-size, as it was reported by Wittich et al. [63] for a system of 125 ion pairs of $[C_4\text{mim}][\text{PF}_6]$. For the solutes, various models were employed. For hydrogen, the potential of Potkowski et al. [64] was used. Potential modes reported by Guillot et al. [65] were employed to describe the noble gases and methane. Nitrogen was described by the Potential of Potoff et al. [66] and oxygen by the Potential of Hansen et al. [67]. Finally, carbon dioxide the EPM2-model of Harris and Yung [68] was used in a modified way as described before [58]. All parameters describing the solutes are give in Table I.

All simulations reported here were performed with the Gromacs simulation program [69]. The preparation of topology files, as well as the data analysis were performed with the most recent version of the MOSCITO suite of

programs [70]. Production runs of 10 ns length were employed for every temperature, starting from previously well equilibrated configurations. The Nosé-Hoover thermostat [71, 72] and the Parrinello-Rahman barostat [73, 74] with coupling times $\tau_T = 1.0$ ps and $\tau_p = 2.0$ ps were used to control constant temperature and pressure (1 bar) conditions. The electrostatic interactions were treated by particle mesh Ewald summation [75]. A real space cutoff of 1.2 nm was employed, and a mesh spacing of approximately 0.12 nm (4th order interpolation) had been used to determine the reciprocal lattice contribution. The Ewald convergence parameter was set to a relative accuracy of the Ewald sum of 10^{-5} . Lennard-Jones cutoff corrections for energy and pressure were considered. A 2 fs timestep was used in all simulations, and every 25th steps a configuration was saved. Distance constraints were solved by means of the SHAKE procedure [76]. The thermodynamic properties of the simulated ionic liquids are essentially identical to the properties reported in Ref. [58].

Infinite Dilution Properties

The solubility of a solute A in a solvent B is conveniently described by the Ostwald coefficient $L^{l/g} = \rho_A^l / \rho_A^g$, where ρ_A^l and ρ_A^g are the number densities of the solute in the liquid and the gas phase of component B, respectively, when both phases are in equilibrium. Alternatively, the solubility of solute A can be expressed in terms of the inverse Henry’s constant k_H^{-1} . The relationship between Henry’s constant and the excess chemical potential $\mu_{\text{ex},A}^l$ in the liquid phase is given by [77]

$$k_H^{-1} = \exp[-\beta \mu_{\text{ex},A}^l] / (\rho_{\text{IL}}^l RT), \quad (1)$$

where $\beta = 1/k_B T$ and ρ_{IL}^l represents the number density of ion pairs in the IL solvent.

According to Widom’s potential distribution theorem [78, 79], the excess chemical potential μ_{ex} can be computed as volume weighted ensemble average

$$\mu_{\text{ex}} = -k_B T \ln \langle V \exp(-\beta \Phi) \rangle / \langle V \rangle. \quad (2)$$

Here V is the volume of the simulation box, and Φ is the energy of a gas molecule inserted at a random position with a random orientation. The brackets $\langle \dots \rangle$ indicate isothermal-isobaric averaging over many configurations, as well as averaging over many insertions.

As control, we also determine the excess chemical potential from energy histograms [80, 81] computed for the energy change $\Delta U = U(N+1) - U(N)$ associated with the insertion $p_0(\Delta U)$ and removal $p_1(\Delta U)$ of a $(N+1)$ th gas molecule from the constant pressure (NPT) simulation. The two distribution functions are related accord-

ing to

$$p_1(\Delta U) = \frac{Q(N, P, T)}{Q(N+1, P, T)} \frac{\langle V \rangle}{\Lambda^3} \times \exp(-\beta \Delta U) p_0(\Delta U), \quad (3)$$

using the definition of the *ideal* and *excess* part of the chemical potential μ referring to the ideal gas state with the same average number density [82], a relation between the two distribution functions and the excess chemical potential is obtained, which is analogous to the expression for the canonical ensemble [82]

$$\ln p_1(\Delta U) - \ln p_0(\Delta U) = \beta \mu_{\text{ex}} - \beta \Delta U. \quad (4)$$

The only difference is the necessity of *volume-weighting* in the calculation of the $p_0(\Delta U)$ -distribution function [83]. For reasons of convenience we define functions f_0 and f_1 according to

$$f_0(\Delta U) = \beta^{-1} \ln p_0(\Delta U) - \frac{\Delta U}{2}, \quad \text{and}$$

$$f_1(\Delta U) = \beta^{-1} \ln p_1(\Delta U) + \frac{\Delta U}{2},$$

such that

$$\mu_{\text{ex}} = f_1(\Delta U) - f_0(\Delta U). \quad (5)$$

All computed energies are based on the minimum image and include a reaction field correction similar to Roberts and Schnitker [84]. Cut-off corrections for the dispersion interactions are included [85].

A total of 2×10^5 configurations were analysed for each IL and for every temperature. Each configuration was sampled by 10^3 random insertions to determine the f_0 -functions. The energies computed for those insertions has also been used to determine “Widom-estimates” for the excess chemical potentials. We would like to point out that the values computed from particle insertions are found to lie within the statistical uncertainty of the data from the overlapping distribution theory. Note that the choice of the sampling rate is a critical parameter for successfully computing the chemical potentials via Widom’s insertion technique. By reducing the sampling rate significantly, we denote a systematic deviation of the “Widom-estimate” from the data obtained via the overlapping distribution method. This effect was observed by us for sampling rates being about two orders of magnitude lower than the rates reported here. All “converged” computed Henry coefficients are shown in Table II.

From the temperature dependence of the computed solvation free energy for infinite dilution, we can comment on the behavior of the first and second derivatives of free energy with respect to temperature. So the solvation entropies, enthalpies, and heat capacities are obtained from fits of the data to a second order expansion of the

solvation free energy around reference state ($T^\circ = 298$ K at $P^\circ = 1$ bar) according to

$$\mu_{\text{ex}}(T) = \mu_{\text{ex}}^\circ - s_{\text{ex}}^\circ(T - T^\circ) - c_{P,\text{ex}}[T(\ln T/T^\circ - 1) + T^\circ]. \quad (6)$$

Here μ_{ex}° and s_{ex}° represent the solvation free energy and solvation entropy at the reference state, respectively. According to the second order expansion, the solvation heat capacity $c_{P,\text{ex}}$ is assumed to be constant over the considered temperature range. The fitted parameters are provided in Table III.

RESULTS AND DISCUSSION

We have computed the solvation free energies μ_{ex} and the associated Henry constants k_{H} for CO_2 , O_2 , N_2 , CH_4 , Kr, Ar, Ne and H_2 at infinite dilution from MD simulations for the four Ionic Liquids $[\text{C}_n\text{mim}][\text{NTf}_2]$ with $n = 2, 4, 6, 8$, employing the sampling techniques discussed in the previous section. The density data for the simulated ionic liquids, necessary to interconvert Henry constants k_{H} and solvation free energies μ_{ex} can be found in Ref. [58]. All computed Henry constants are summarised in Table II. The temperature dependence of the corresponding solvation free energies $\mu_{\text{ex}}(T)$ has been fitted to a second order expansion around a reference state following Eq. 6. The parameters obtained for a reference temperature of $T^\circ = 298$ K are given in Table III. In Figure 2 a section of computed solubilities (here given as inverse Henry’s constants) are compared with available experimental and theoretical data. For reasons of clarity, we restrict this comparison to data based on solvation in $[\text{C}_6\text{mim}][\text{NTf}_2]$. Most experimental data sets are only available for this particular IL, since it had been selected as the reference compound for an IUPAC experimental validation project [87, 88]. The remainder of this section is organised as follows: First we will compare our simulated solubility data with available experimental and theoretical data. A short discussion of the available solubility data is given for every gas in detail. The following sections will then focus on a systematic rationalization of the effect of varying the alkane chain length, and of changing the temperature by introducing the concept of the “solvation funnel”.

Comparison with Available Experimental and Theoretical Data

Carbon Dioxide

For carbon dioxide we have shown previously [58] that all available experimental and theoretical data are in excellent agreement with our simulation results. Particularly, the temperature dependence is reflected very well

by the simulations [16, 18, 89, 90]. Moreover, we could recently show that small differences with respect to a few experimental data sets could be explained by water content in the samples [91]. The data calculated for CO_2 by Sumon et al. [30] using COSMO-RS, and Wu et al. [51], as well as Shi et al. [38] using molecular simulation techniques, show the same temperature trend for carbon dioxide and are all very close to the experimental data.

Methane

Experimental data for the solubility of methane are available from various sources. Kumelan et al. [49] have examined methane in $[\text{C}_6\text{mim}][\text{NTf}_2]$ over a large temperature range. In addition, the data of Finotello et al. [16] are shown, who investigated $[\text{C}_2\text{mim}][\text{NTf}_2]$ and $[\text{C}_6\text{mim}][\text{NTf}_2]$. Moreover, we also show the data according to Camper et al. [92], as well as Anderson et al. [93], and Blath et al. [94] for $[\text{C}_6\text{mim}][\text{NTf}_2]$. Our data predict a systematically higher solubility compared with the mostly consistent experimental data sets, but are well in agreement with the temperature slope of the data of Kumelan et al. The temperature dependencies reported by Finotello and Anderson, however, are clearly not compatible with our findings and the data of Kumelan et al. We would like to point out, that we did not perform any adjustment to the force field parameters to improve the solute-solvent interaction. The Lennard-Jones parameters of Guillot et al. apparently overestimate the interaction between the solvent and solute. The data calculated for CH_4 by Sumon et al. using COSMO-RS [30] show the same temperature trend for methane as our simulations.

Noble Gases

For the case of krypton there is only one experimental dataset available, published by Afzal et al. [95] in 2013 (not shown here). It shows the same temperature trend as our simulated results. For the case of argon and neon are, to our knowledge, no experimental data available. In 2010 Shi et al. [52] published Henry constants obtained from computer simulations of argon in $[\text{C}_6\text{mim}][\text{NTf}_2]$. Their data are in the same decade compared to ours, and the temperature dependence is similar, but their computed solubilities are slightly smaller.

Oxygen

For the case of oxygen, there are only few experimental solubility data sets available. This is likely due to the experimental challenges associated with the use of oxygen. Our data apparently slightly overestimates the solubility of oxygen, but seems to agree par-

TABLE II: Calculated Henry constants k_H for various gaseous components dissolved in in imidazolium based ionic liquids of type $[C_n \text{mim}][\text{NTf}_2]$. All data were obtained from MD simulations at 1 bar and describe the infinite dilution limit according to $k_H = \exp[\beta \mu_{\text{ex,Gas}}^l] \times \rho_{\text{IL}}^l RT$ [77]. The ion-pair densities are computed from fitted second order polynomial ρ_{IL}^l [86].

T/K		k_H/bar			
		$[\text{C}_2\text{mim}]$	$[\text{C}_4\text{mim}]$	$[\text{C}_6\text{mim}]$	$[\text{C}_8\text{mim}]$
CO_2	300	34±3	28±3	29±3	22±3
	350	87±6	73±5	63±4	56±6
	400	140±8	121±6	107±6	98±9
	450	207±10	171±9	152±8	139±11
	500	262±12	224±11	191±9	185±13
Kr	300	188±5	143±6	119±6	89±6
	350	266±4	210±3	175±2	139±3
	400	327±3	261±3	221±2	182±3
	450	377±2	306±2	257±1	214±1
	500	411±2	337±3	284±2	240±1
CH_4	300	300±10	224±15	214±15	142±10
	350	381±7	300±7	277±6	203±5
	400	441±3	351±4	321±4	249±3
	450	486±5	391±3	353±3	278±2
	500	509±4	415±3	373±3	299±2
Ar	300	436±9	350±12	318±14	242±15
	350	508±6	418±6	378±4	303±6
	400	548±4	455±5	410±4	340±4
	450	571±3	478±3	427±2	356±2
	500	577±2	486±3	431±3	365±2
O_2	300	652±22	523±21	456±23	378±26
	350	720±7	596±8	517±5	447±10
	400	744±5	619±7	540±5	480±6
	450	750±5	629±4	545±3	482±3
	500	732±4	621±5	536±3	477±3
N_2	300	1048±47	858±42	766±46	651±53
	350	1062±15	898±14	795±12	707±20
	400	1036±7	875±11	775±9	703±11
	450	991±8	844±7	741±4	666±6
	500	942±4	802±7	699±4	629±5
Ne	300	3418±63	3051±88	2898±110	2752±172
	350	2507±23	2222±25	2088±16	1964±36
	400	1943±13	1716±10	1587±13	1480±8
	450	1570±12	1388±8	1267±5	1185±10
	500	1318±6	1147±5	1047±5	977±7
H_2	300	3875±98	3286±121	3313±157	2718±173
	350	2867±42	2466±44	2415±33	2066±42
	400	2216±16	1906±23	1835±19	1610±21
	450	1805±22	1552±10	1462±7	1279±9
	500	1510±5	1296±10	1190±13	1058±8

ticularly well with the slope of the temperature dependence reported by Kumelan et al. [96] in $[\text{C}_6\text{mim}][\text{NTf}_2]$. The temperature dependent data of Anthony et al. [97] for $[\text{C}_4\text{mim}][\text{NTf}_2]$ (not shown here), however, suggest

a significantly stronger temperature dependence, in accordance with the recently published values of Afzal et al. [95]. The simulation-based data of Shi et al. [38] seem to be placed right in the middle between the data

TABLE III: Thermodynamic parameters describing the temperature dependence of the solvation free energies $\mu_{\text{ex}}(T)$ of the indicated solutes according to a second order expansion around a thermodynamic reference state, following Eq. 6. The chosen reference state has been set to $T^\circ = 298 \text{ K}$ at $P^\circ = 1 \text{ bar}$.

		[C ₂ mim]	[C ₄ mim]	[C ₆ mim]	[C ₈ mim]
CO ₂	$\mu_{\text{ex}}^\circ/\text{kJ mol}^{-1}$	-2.57	-2.79	-2.45	-2.89
	$s_{\text{ex}}^\circ/\text{JK}^{-1} \text{ mol}^{-1}$	-39.1	-40.1	-33.8	-39.2
	$h_{\text{ex}}^\circ/\text{kJ mol}^{-1}$	-14.2	-14.7	-12.5	-14.6
	$c_{P,\text{ex}}/\text{JK}^{-1} \text{ mol}^{-1}$	45	48	34	43
Kr	$\mu_{\text{ex}}^\circ/\text{kJ mol}^{-1}$	1.66	1.24	1.09	0.56
	$s_{\text{ex}}^\circ/\text{JK}^{-1} \text{ mol}^{-1}$	-20.5	-21.3	-20.9	-23.1
	$h_{\text{ex}}^\circ/\text{kJ mol}^{-1}$	-4.45	-5.09	-5.13	-6.32
	$c_{P,\text{ex}}/\text{JK}^{-1} \text{ mol}^{-1}$	19.9	21.9	21.7	26.8
CH ₄	$\mu_{\text{ex}}^\circ/\text{kJ mol}^{-1}$	2.78	2.36	2.55	1.73
	$s_{\text{ex}}^\circ/\text{JK}^{-1} \text{ mol}^{-1}$	-18.5	-19.7	-18.4	-21.8
	$h_{\text{ex}}^\circ/\text{kJ mol}^{-1}$	-2.72	-3.50	-2.92	-4.76
	$c_{P,\text{ex}}/\text{JK}^{-1} \text{ mol}^{-1}$	17.6	20.8	18.6	27.0
Ar	$\mu_{\text{ex}}^\circ/\text{kJ mol}^{-1}$	3.76	3.48	3.54	3.06
	$s_{\text{ex}}^\circ/\text{JK}^{-1} \text{ mol}^{-1}$	-16.2	-16.7	-16.6	-18.4
	$h_{\text{ex}}^\circ/\text{kJ mol}^{-1}$	-1.07	-1.51	-1.42	-2.41
	$c_{P,\text{ex}}/\text{JK}^{-1} \text{ mol}^{-1}$	16.9	18.4	19.3	23.5
O ₂	$\mu_{\text{ex}}^\circ/\text{kJ mol}^{-1}$	4.76	4.48	4.43	4.17
	$s_{\text{ex}}^\circ/\text{JK}^{-1} \text{ mol}^{-1}$	-16.8	-17.2	-17.1	-19.0
	$h_{\text{ex}}^\circ/\text{kJ mol}^{-1}$	-0.23	-0.66	-0.67	-1.50
	$c_{P,\text{ex}}/\text{JK}^{-1} \text{ mol}^{-1}$	19.0	20.0	20.7	26.0
N ₂	$\mu_{\text{ex}}^\circ/\text{kJ mol}^{-1}$	5.95	5.72	5.73	5.53
	$s_{\text{ex}}^\circ/\text{JK}^{-1} \text{ mol}^{-1}$	-15.5	-16.4	-16.2	-18.4
	$h_{\text{ex}}^\circ/\text{kJ mol}^{-1}$	1.34	0.84	0.90	0.04
	$c_{P,\text{ex}}/\text{JK}^{-1} \text{ mol}^{-1}$	17.0	20.0	21.0	27.6
Ne	$\mu_{\text{ex}}^\circ/\text{kJ mol}^{-1}$	8.89	8.90	9.07	9.13
	$s_{\text{ex}}^\circ/\text{JK}^{-1} \text{ mol}^{-1}$	-5.66	-5.91	-5.36	-4.96
	$h_{\text{ex}}^\circ/\text{kJ mol}^{-1}$	7.20	7.14	7.47	7.65
	$c_{P,\text{ex}}/\text{JK}^{-1} \text{ mol}^{-1}$	10.1	12.3	11.7	10.8
H ₂	$\mu_{\text{ex}}^\circ/\text{kJ mol}^{-1}$	9.19	9.09	9.40	9.11
	$s_{\text{ex}}^\circ/\text{JK}^{-1} \text{ mol}^{-1}$	-7.29	-7.72	-7.29	-8.99
	$h_{\text{ex}}^\circ/\text{kJ mol}^{-1}$	7.02	6.79	7.23	6.43
	$c_{P,\text{ex}}/\text{JK}^{-1} \text{ mol}^{-1}$	11.3	13.4	14.9	19.0

of Afzal et al. and Kumelan et al.

Nitrogen

The solubility of nitrogen has been studied by several groups. Unfortunately, the temperature trends of the available experimental and theoretical data sets seem to be quite inconsistent. The data of Camper et al. [92] and Finotello et al. [16] in [C₂mim][NTf₂] and [C₆mim][NTf₂], as well as Blath et al. [94] (measured at 60°C in [C₆mim][NTf₂]) are very close with respect to each other. Our data is in the same range as the experimental data, however, we do not observe a significant in-

crease of the computed solubilities with increasing temperature. Both, the data calculated for N₂ by Sumon et al. [30] using COSMO-RS [30], and Shi et al. [38] using computer simulation techniques show a significantly different temperature dependence compared to the experimental data sets of Finotello et al.

Hydrogen

For the solubility of molecular hydrogen, experimental data from various groups are available. However, different groups report substantially different, inconsistent results. The group of Costa Gomes [17, 18] has stud-

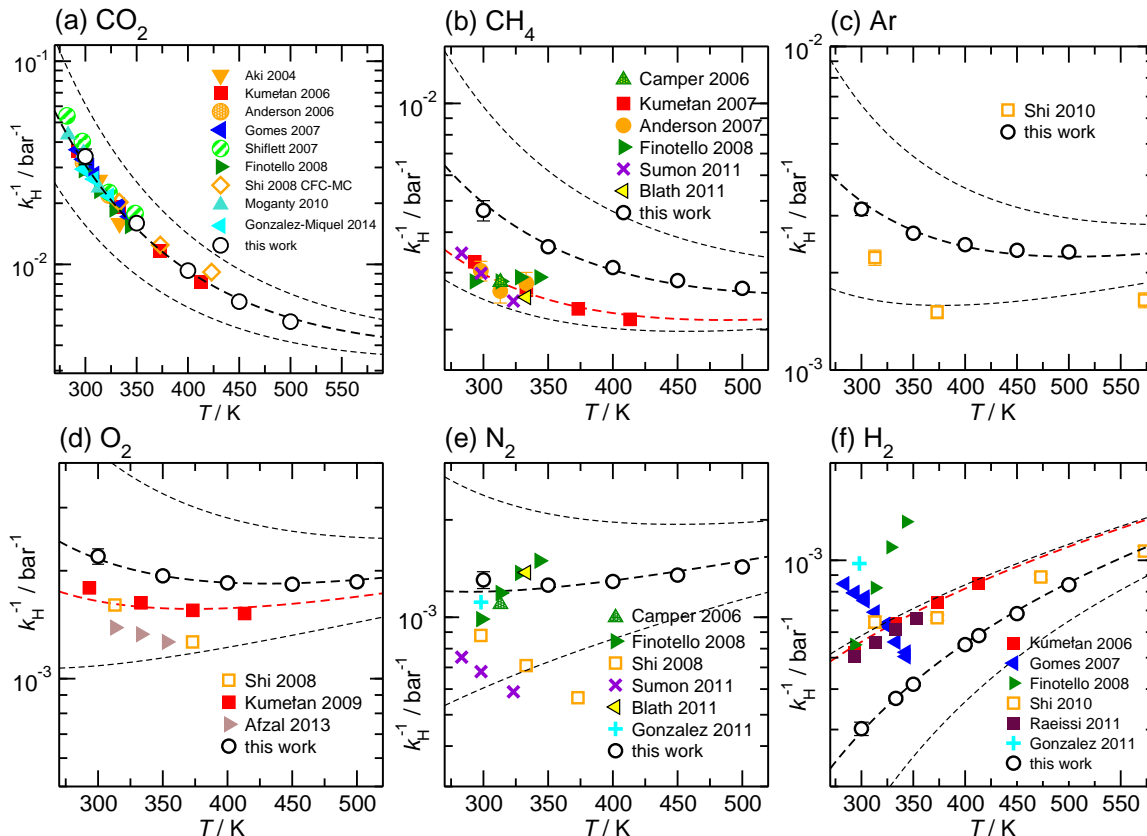


FIG. 2: Solubilities $k_H^{-1} = \exp[-\beta \mu_{ex, Gas}^I] / \rho_{IL} RT$ of selected gases in in $[C_6mim][NTf_2]$. Shown are data for a) CO_2 , b) CH_4 , c) Ar, d) O_2 , e) N_2 , and f) H_2 at 1 bar. The filled symbols represent experimental data given according to the indicated sources. Open symbols specify data from to molecular simulations, while crosses represent data obtained from alternative theoretical predictions. All dashed lines show theoretical predictions based on our “solvation funnel” model. The upper and lower black thin dashed lines are temperature-predictions for solubilities twice and half of the reference-value used for our MD simulation-data (given as black thick dashed line). The red dashed line represents a “solvation funnel prediction” for the experimental solubility data of Kumelan et al. References for the experimental and theoretical data are given in the text.

ied $[C_2mim][NTf_2]$, $[C_4mim][NTf_2]$ and $[C_6mim][NTf_2]$ and found decreasing solubility with increasing temperature. Dyson et al. [20] just published one value for $[C_4mim][NTf_2]$. In stark contrast to the findings of Costa Gomes, Finotello et al. [16], who examined $[C_2mim][NTf_2]$ and $[C_6mim][NTf_2]$, found a strongly increasing solubility with increasing temperature. Kumelan et al. [98] observed this trend as well for $[C_6mim][NTf_2]$, albeit with a significantly weaker temperature dependence. The experimental data of Raeissi et al. [26] seem to match almost exactly the data of Kumelan et al. Shi et al. [52] published Henry constants for hydrogen in $[C_6mim][NTf_2]$ from computer simulations. Their results support our result of a positive slope of the temperature dependent solubility data and match very well the values of Kumelan et al. [98] as well as Raeissi et al. [26].

Alkane Chain-Length Dependence

The computed solubilities as a function of the alkane chain length obtained from MD simulation are given as inverse Henry coefficients, and are shown as full symbols in Figure 3. The data indicate a rather small variation for ILs with varying chain-length. However, there is a significant tendency towards higher solubilities for gases in ionic liquids with longer alkane chains. When comparing the solubility data for $[C_2mim][NTf_2]$ and $[C_8mim][NTf_2]$ for all the investigated gases, we consistently observe an increase in solubility of about 30% to 40% for the component with the C8-chain. In Ref. [58] we reported the observation that the solvation free energies μ_{ex} of carbon dioxide showed almost no chain-length dependence at a given temperature. By assuming μ_{ex} to be chain-length independent, it follows that the chain-length dependence of the solubility data at a given temperature can be solely expressed due to density scaling according to Equation

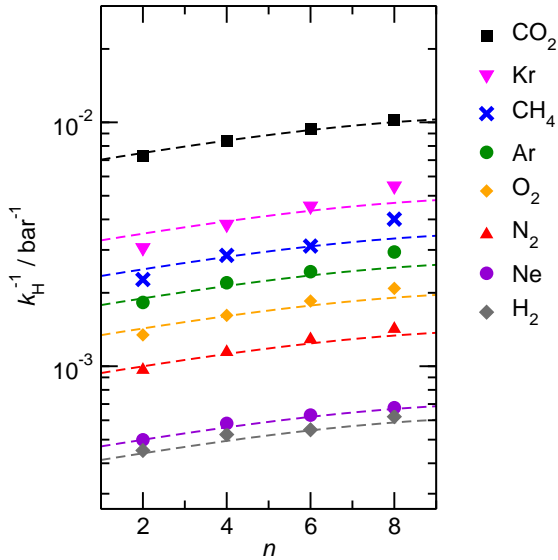


FIG. 3: Comparison of inverse Henry constants of all simulated gases in $[C_n\text{mim}][\text{NTf}_2]$ with varying chain lengths $n=2, 4, 6, 8$ at 400 K. The dashed lines are predictions of the chain-length dependence based on the density-scaling procedure described by Equation 7.

1, leading to an approximate expression:

$$k_{\text{H}}^{-1}(\rho'_{\text{IL}}) \approx k_{\text{H}}^{-1}(\rho_{\text{IL}}) \times \frac{\rho_{\text{IL}}}{\rho'_{\text{IL}}}, \quad (7)$$

where ρ_{IL} and ρ'_{IL} represent the number densities of the ion pairs in ionic liquids with different alkane chain lengths. Using the density data of our simulated ionic liquids (data is given in Ref. [58]), we have fitted the number density as a function of chain length n to a second order polynomial:

$$\rho_{\text{IL}}(n) = \rho_{\text{IL}}^{(0)} + \rho_{\text{IL}}^{(1)} \cdot n + \rho_{\text{IL}}^{(2)} \cdot n^2 \quad (8)$$

with $\rho_{\text{IL}}^{(0)} = 2.406 \text{ nm}^{-3}$, $\rho_{\text{IL}}^{(1)} = -0.1584 \text{ nm}^{-3}$, and $\rho_{\text{IL}}^{(2)} = 6.39 \times 10^{-3} \text{ nm}^{-3}$ for $T = 400 \text{ K}$. As shown in Figure 3, the rather simple density scaling procedure describes rather accurately the chain-length dependence of the solubility-data of the entire set of gases, suggesting that the condition $\mu_{\text{ex}}(n) \approx \text{const.}$ is mostly fulfilled for those gases.

Temperature Dependence: “Solvation Funnel”

From the wealth of experimental and theoretical solubility data presented in Figure 2 (including our data) we conclude that there apparently exists a systematic relation between the temperature dependent slope of the solubilities of different gases and their interaction-strength with the solvent: Rather “strongly” interacting species,

such as CO_2 , show apparently a strong “anomalous” temperature dependence of the solubility, whereas weakly interacting species such as oxygen and argon show a significantly weaker temperature behavior. Finally, for the case of molecular hydrogen H_2 , we observe a change in sign of the slope, showing a strongly increasing solubility with increasing temperature. The latter finding is apparently supported by the majority of experimental data sets. However, for two cases, namely nitrogen and hydrogen, there are substantially conflicting results from different sources, each suggesting a very different kind of temperature behavior. How could this be resolved? We think that the apparent systematic trend is deeply rooted in the free energy landscape explored by a solvated gas molecule, and that the observed trend can be explained by purely thermodynamic means.

By fitting the temperature dependent solvation free energies $\mu_{\text{ex}}(T)$ to the second order expansion around a thermodynamic reference state ($T^\circ = 298 \text{ K}$ and $P^\circ = 1 \text{ bar}$) given by Eq. 6, we obtain standard solvation free energies μ_{ex}° , entropies s_{ex}° , enthalpies h_{ex}° , as well as the solvation heat capacities $c_{P,\text{ex}}^\circ$. Data computed for all studied gases and ionic liquids are collected in Table III. In addition, we also consider data for a modified CO_2 molecule, where we have systematically weakened the interaction with the solvent by switching off the Coulomb interaction, and by scaling the Lennard-Jones interaction using a factor f with $\varepsilon_{ij} = (f\varepsilon_{ii}\varepsilon_{jj})^{1/2}$. Finally, this prototypical molecule is transformed into a purely repulsive component by modelling the solute-solvent interaction solely via Weeks-Chandler-Andersen-type (WCA) interactions according to $V_{ij}(r) = V_{ij,\text{LJ}}(r) + \varepsilon_{ij}$ for $r \leq r_{\text{LJ},\text{min}}$, and $V_{ij}(r) = 0$ otherwise. Following the procedure suggested by Simha et al. for the dissolution of gases in polymers [99, 100], Figure 4a shows a plot of the standard solvation free energy μ_{ex}° vs. the solvation enthalpy h_{ex}° for all studied gases in all solvents. It is evident, that both properties are linearly related for the entire set of solvation data. This linear relationship can be utilized to predict the temperature dependent solvation data. Furthermore, it can provide us with a quantitative representation of the notion that the absolute solubility of a certain compound and its temperature behavior are somehow related. The thermodynamic definition of the free energy implies that the solvation entropy and enthalpy have to be linearly related as well, as it is demonstrated in Figure 4b. To quantify the relations shown in Figure 4 we use the following relation:

$$h_{\text{ex}}^\circ = a \cdot \mu_{\text{ex}}^\circ + b, \quad (9)$$

with $a = 1.653$ and $b = -7.87 \text{ kJ mol}^{-1}$, representing the parameters used for plotting the dashed lines shown in Figure 4a and 4b. From equation 9 follows the relation between s_{ex}° and h_{ex}° as

$$T^\circ s_{\text{ex}} = h_{\text{ex}}^\circ \cdot \frac{a-1}{a} + \frac{b}{a}. \quad (10)$$

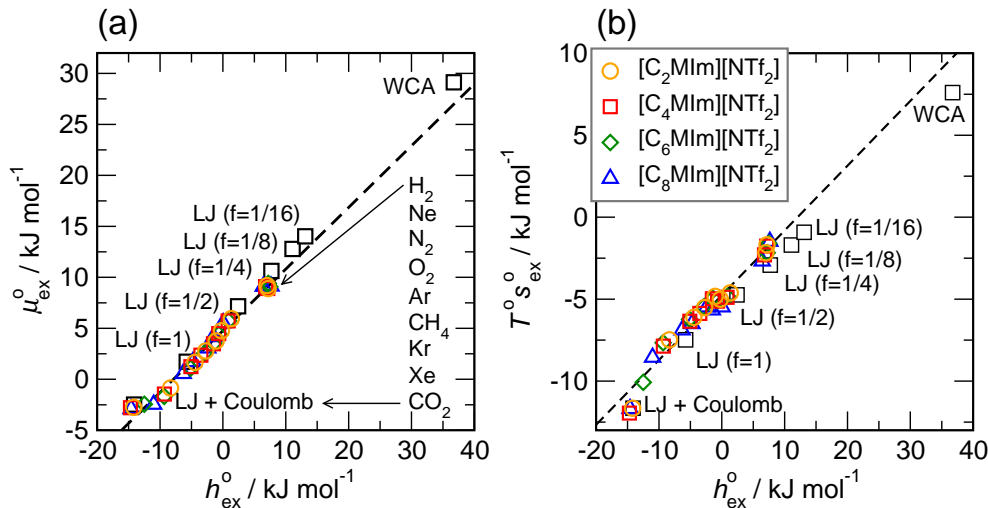


FIG. 4: (a) Correlation between the solvation free energy μ_{ex}° and the solvation enthalpy h_{ex}° for gases dissolved in $[\text{C}_n\text{mim}][\text{NTf}_2]$ at the reference state. (b) Correlation between the solvation entropy s_{ex}° and the solvation enthalpy h_{ex}° . Shown are data for all other examined gases (colored) as well as the scaled potential model variants of CO₂ (black squares), taken from Ref. [58]

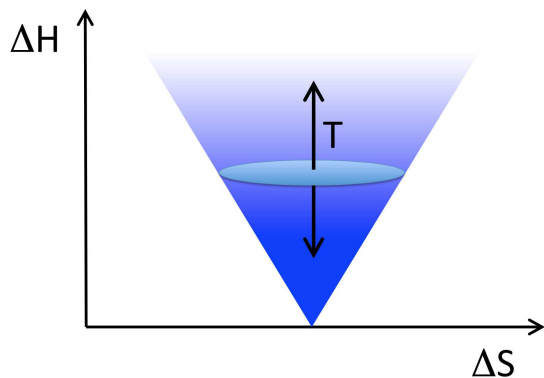


FIG. 5: Schemetical representation of a hypothetical funnel-like free energy landscape of a light gas molecule dissolved in an ionic liquid. The gas molecule explores few low energy states and many high energy states, leading to a positive correlation between the solvation free energy and the solvation enthalpy.

The excellent correlation between s_{ex}° and h_{ex}° over a rather wide range of interaction strengths is apparently intimately related to the process of solvation of small gas molecules. In particular, how a gas molecule and its solvation shell explore the configurational space of the solvated state. To rationalize this behavior, Figure 5 provides a graphical representation of a hypothesized funnel-like free energy landscape of a solvated light gas molecule. Consequently, we call this concept “solvation funnel”, not unlike the “folding funnel” used to describe the free energy landscape and the thermodynamic behavior of organised polymers such as proteins [101]. The solvated gas molecule is thought to explore few low energy states and many high energy states, leading to a funnel-like free en-

ergy landscape. The consequence is a positive correlation between the solvation entropy and the solvation enthalpy. By scaling up the interaction of the gas with the solvent, low energy states are more strongly weighted, hence the funnel is deepened. Changing the temperature, basically changes the population of states in the funnel-like landscape. We would like to point out that by restricting our study to “small gas molecules”, the variation in size of the molecules has apparently no big effect, and is being accounted for effectively. For larger solutes this might not necessarily be the case.

The relation between s_{ex}° and μ_{ex}° as outlined above, essentially determines the coupling between the absolute solubility and its temperature dependence. However, the second order expansion of $\mu_{\text{ex}}(T)$ given in Eq. 6 requires also the knowledge of the heat capacity of solvation $c_{P,\text{ex}}$, to fully determine the temperature dependence of all our solubility data. Fortunately, the variation of the computed $c_{P,\text{ex}}$ -values, given in Table III, and shown in Figure 6, has no big effect. If we neglect the heat capacity contribution completely by setting $c_{P,\text{ex}} = 0$, we arrive at a description, which is qualitatively correct for all investigated gases (not shown). This procedure, however, leads to significant deviations of the predicted data from our simulation data for temperatures above 400 K. A much better description is achieved by using a common value of $c_{P,\text{ex}} = 20 \text{ J K}^{-1} \text{ mol}^{-1}$ for all gases instead, as it is indicated by the predictions represented by thin dashed lines in Figure 7. However, to improve things further, we make use of a negative correlation between μ_{ex}° and $c_{P,\text{ex}}$, suggested by Figure 6. To complete our “solvation-funnel”-model we make use of the linear relationship between μ_{ex}° and $c_{P,\text{ex}}$:

$$c_{P,\text{ex}} = c \cdot \mu_{\text{ex}}^{\circ} + d \quad (11)$$

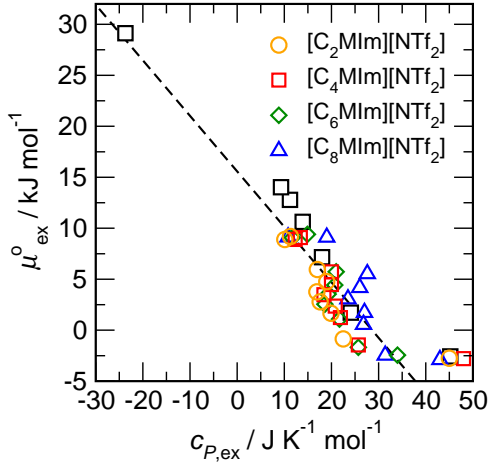


FIG. 6: Correlation between the solvation free energy μ_{ex}^0 and the solvation heat capacity $c_{P,\text{ex}}$ dissolved in $[\text{C}_n\text{mim}][\text{NTf}_2]$ obtained for the different potential model variants of CO_2 (black) [58] and for all other examined gases (colored) at standard conditions.

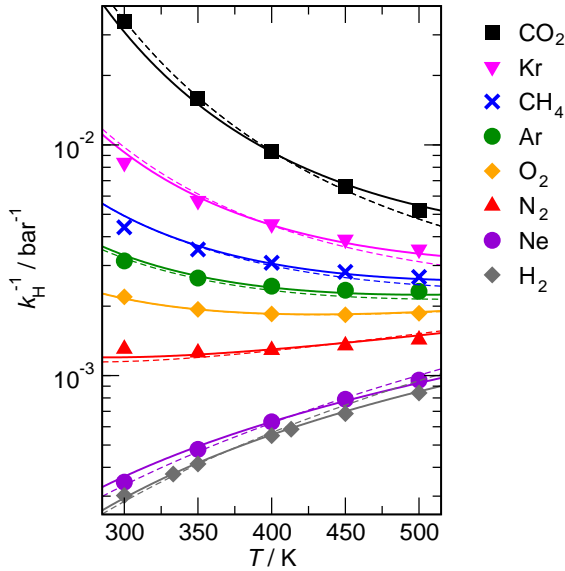


FIG. 7: The symbols denote the temperature dependence of the inverse Henry constants for all simulated gases dissolved in $[\text{C}_6\text{mim}][\text{NTf}_2]$. The lines indicate the predictions of the “solvation funnel” model. Thin dashed lines: $c_{P,\text{ex}} = 20 \text{ J K}^{-1} \text{ mol}^{-1}$. Heavy solid lines: $c_{P,\text{ex}}$ according to Eq. 11.

with $c = -1.837 \cdot 10^{-3} \text{ K}^{-1}$ and $d = 28.621 \text{ J mol}^{-1} \text{ K}^{-1}$. With just four parameters, it is now possible to quantitatively predict the temperature dependence of the solubility of all studied gases in all four solvents. The only requirement is the knowledge of the solubility of a gas at the reference temperature T° . These “solvation funnel” model predictions with variable $c_{P,\text{ex}}$ are represented by thick solid lines in Figure 7 for all studied gases. In addition to the temperature dependent experimental data,

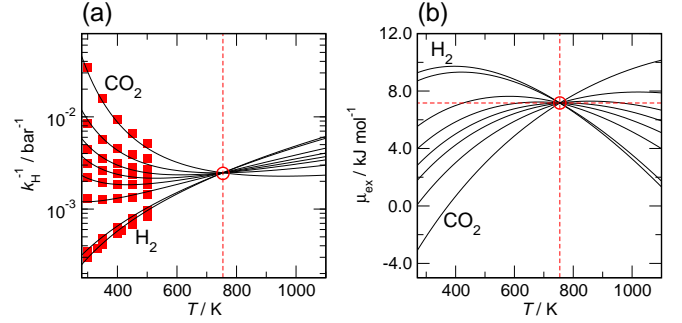


FIG. 8: “Solvation funnel” model predictions for all gases in $[\text{C}_6\text{mim}][\text{NTf}_2]$ with a constant $c_{P,\text{ex}} = 20 \text{ J K}^{-1} \text{ mol}^{-1}$. Indicated is the intersection temperature $T^* = 754.4 \text{ K}$. (a) Predicted solubilities. Red squares indicated experimental solubilities. (b) Predicted solvation free energies $\mu_{\text{ex}}(T)$.

we have included predictions according to our “solvation funnel” model also in Figure 2. The thick dashed lines in Figure 2 represent data chosen to match our simulation data. The thin dashed lines are used to illustrate the temperature evolution of the model predictions in the vicinity of one particular solute. Here reference solubilities were chosen to be half and twice the size of the reference-solubility used for matching our MD simulation data. It is quite evident that particularly for N_2 , and H_2 several experimental data-sets are incompatible with our model predictions. However, the red dashed lines shown in Figure 2 demonstrate that the experimental data obtained by the Maurer group in Kaiserslautern (the data of Kumelán et al. are represented by red symbols in Figure 2a,2b,2d, and 2f) for a variety of solutes are consistently in very good agreement with the predictions of the “solvation funnel” model. This includes even the controversial case of molecular hydrogen.

Finally, we would put another argument forward, that a positive slope for the temperature dependence of the hydrogen-solubility data is a very likely scenario. Following the arguments of Hayduk and Laudie [102], which have been reviewed and extended by Beutier and Renon [103], all Henry constants and hence all solubilities obtained for a certain solvent should meet at the critical point of that solvent, in our case the ionic liquids. The solubility data shown in Figure 7 clearly indicate a convergent behavior with increasing temperature. By extrapolating the “solvation funnel” model to very high temperatures, we find that this convergence even continues. In addition, Figure 8 demonstrates that by assuming $c_{P,\text{ex}}$ to be constant, the “solvation funnel” model even predicts a single common intersection temperature T^* for the solubility all gases. Equations 6 and 9 imply that the common temperature T^* is defined by

$$T^* = T^\circ \cdot \frac{a}{a-1} \quad (12)$$

with the corresponding common solvation free energy of

$$\mu_{\text{ex}}(T^*) = \frac{b}{1-a} + \frac{c_{P,\text{ex}}T^\circ}{1-a} \left[a \cdot \ln\left(\frac{a}{a-1}\right) - 1 \right]. \quad (13)$$

It is remarkable that Equation 12 just requires the knowledge of the parameter a , defined in Equation 9, as well as the chosen reference temperature T° . By using $a = 1.653$ and $T^\circ = 298$ K, we compute a common temperature of $T^* = 754.4$ K for all gases used in this study. The solubility curves intersect at a value of $\mu_{\text{ex}}(T^*) = 7.166$ kJ mol⁻¹ for the case of $c_{P,\text{ex}} = 20$ J K⁻¹ mol⁻¹ (indicated in Figure 8). However, by allowing $c_{P,\text{ex}}$ to vary slightly for each gas, this constraint of a common temperature is violated. This does not necessarily mean that our model is inadequate, but rather that the temperature range of our study is too far away from the critical temperature. It is not unlikely that, by approaching the critical point, the solvation heat capacities $c_{P,\text{ex}}$ will eventually converge, while the solvated gases maintain their solvation enthalpy-entropy correlation. This would again restore the common temperature feature. Although the predicted solubility-data with variable $c_{P,\text{ex}}$ do not meet exactly at a particular temperature, they show a region of nearest approximation around 1100 K, which is far above the decomposition point of any of the ionic liquids. We would like to point out, however, that this coincides nicely with results from Rebelo et al. [104] and Freire et al. [105], who estimated the location of the critical temperature to be around 1100 K using surface tension data in combination with the Eötvös and Guggenheim equations. Their predicted critical temperature, however, was significantly larger than the predictions of Yokozeki et al. [106], who used the Vetere method, as well as of Shin et al. [107], who used the group contribution method (GCM) of Joback, and Valderrama et al. [108], who obtained results applying the modified Lydersen-Joback-Reid method (mLJR).

CONCLUSION

The systematic behavior of the gas solubility in Ionic Liquids is studied and described with the help of extensive molecular dynamics simulations. The solubility of hydrogen, oxygen, nitrogen, methane, krypton, argon, neon and carbon dioxide in the Ionic Liquids of type 1-*n*-alkyl-3-methylimidazolium bis(trifluoromethylsulfonyl)imide ([C_{*n*}mim][NTf₂]) with varying chain lengths $n = 2, 4, 6, 8$ are computed for a large temperature range from 300 K up to 500 K at 1 bar. By applying Widom’s particle insertion technique, as well as Bennett’s overlapping distribution method, we are able to determine solvation free energies for those selected light gases in imidazolium based Ionic Liquids with great statistical accuracy. A detailed comparison of

the computed solubility data with available experimental and theoretical data is provided.

We observe, that the chain-length dependence of the computed solubility in various solvents can be mostly attributed to the change of the number-density of ion-pairs in the solvent, as the computed solvation free energies show almost no chain-length dependence.

The data obtained from our MD simulations clearly show that the magnitude of the solvation free energy at a defined reference temperature and its temperature-derivatives are intimately related with respect to one-another. This is a consequence of a solvation entropy-enthalpy compensation effect, which seems to be a defining feature of the solvation of small molecules in the investigated Ionic Liquids. We rationalize this feature as the consequence of a hypothesized funnel-like free-energy landscape explored by the solvated gas molecule. This effect is leading to simple analytical relations quantitatively describing the temperature dependent solubility of gases solely depending on the absolute solubility value at a defined reference temperature which we call “solvation funnel” model.

The “solvation funnel” model is also predicting that the solubility data all meet at a single temperature, which is in line with the observation made for various fluids that the solubilities for gases meet at the critical temperature. However, this feature of a common temperature exists only, if the model is used with a unique heat capacity of solvation valid for all gases. Since the computed heat capacities of solvation do not vary strongly for different gases, a common value of $c_{P,\text{ex}} = 20$ J K⁻¹ mol⁻¹ is a reasonable approximation for all investigated solutes.

We would like to point out that the “solvation funnel” model is particularly helpful for assessing the solvation behavior of very light gases, such as hydrogen, where conflicting experimental data have been reported.

ACKNOWLEDGEMENTS

This work has been supported by the German Science Foundation (DFG) priority program SPP 1570 with additional support from SFB 652.

* Electronic address: dkerle@uni-bremen.de

† Electronic address: dietmar.paschek@uni-rostock.de

- [1] P. Wasserscheid, T. Welton, *Ionic Liquids in Synthesis*, 2nd Aufl., VCH-Wiley, Weinheim, **2007**.
- [2] C. A. Angell, Y. Ansari, Z. Zhao, *Faraday Discuss.* **2012**, *154*, 9–27.
- [3] F. Endres, S. Z. El Abedin, *Phys. Chem. Chem. Phys.* **2006**, *8*, 2101–2116.
- [4] R. D. Rogers, K. R. Seddon, *Science* **2003**, *302*, 792–793.

- [5] M. Smiglak, A. Metlen, R. D. Rogers, *Acc. Chem. Res.* **2007**, *40*, 1182–1192.
- [6] N. V. Plechkova, K. R. Seddon, *Chem. Rev.* **2008**, *37*, 123–150.
- [7] L. A. Blanchard, D. Hancu, E. J. Beckman, J. F. Brennecke, *Nature* **1999**, *399*, 28–29.
- [8] D. J. Tempel, P. B. Henderson, J. R. Brzozowski, R. M. Pearlstein, H. Cheng, *J. Am. Chem. Soc.* **2008**, *130*, 400–401.
- [9] J. Huang, T. R  ther, *Aust. J. Chem.* **2009**, *62*, 298–308.
- [10] M. Ramdin, T. W. de Loos, T. J. H. Vlught, *Ind. Eng. Chem. Res.* **2012**, *51*, 8149–8177.
- [11] J. E. Bara, D. E. Camper, D. L. Gin, R. D. Noble, *Acc. Chem. Res.* **2010**, *43*, 152–159.
- [12] S. Raeissi, C. J. Peters, *Green Chem.* **2009**, *11*, 185–192.
- [13] C. Myers, H. Pennline, D. Luebke, J. Ilconich, J. K. Dixon, E. J. Maginn, J. F. Brennecke, *J. Membrane Science* **2008**, *322*, 28–31.
- [14] J. Ilconich, C. Myers, H. Pennline, D. Luebke, *J. Membrane Science* **2007**, *298*, 41–47.
- [15] Z. Lei, C. Dai, B. Chen, *Chem. Rev.* **2013**, *0*, null, DOI 10.1021/cr300497a.
- [16] A. Finotello, J. E. Bara, D. Camper, R. D. Noble, *Ind. Eng. Chem. Res.* **2008**, *47*, 3453–3459.
- [17] J. Jacquemin, P. Husson, V. Majer, M. F. Costa Gomes, *J. Solution Chem.* **2007**, *36*, 967–979.
- [18] M. F. C. Gomes, *J. Chem. Eng. Data* **2007**, *52*, 472–475.
- [19] J. Kumelan, A. P. S. Kamps, D. Tuma, G. Maurer, *J. Chem. Thermodynamics* **2006**, *38*, 1396–1401.
- [20] P. J. Dyson, G. Laurenczy, C. A. Ohlin, J. Vallance, T. Welton, *Chem. Commun* **2003**, ., 2418–2419.
- [21] J. Jacquemin, M. F. Costa Gomes, P. Husson, V. Majer, *J. Chem. Thermodynamics* **2006**, *38*, 490–502.
- [22] J. Jacquemin, P. Husson, V. Majer, A. A. H. Padua, M. F. Costa Gomes, *Green Chem.* **2008**, *10*, 944–950.
- [23] J. Jacquemin, P. Husson, V. Majer, M. F. Costa Gomes, *Fluid Phase Equilibria* **2006**, *1*, 87–95.
- [24] J. Kumelan, A. P. S. Kamps, D. Tuma, G. Maurer, *J. Chem. Eng. Data* **2006**, *51*, 11–14.
- [25] J. Kumelan, D. Tuma, A. P. S. Kamps, G. Maurer, *J. Chem. Eng. Data* **2010**, *55*, 165–172.
- [26] S. Raeissi, L. J. Florusse, C. J. Peters, *J. Chem. Eng. Data* **2011**, *56*, 1105–1107.
- [27] Y. Shimoyama, A. Ito, *Fluid Phase Equilibria* **2010**, *297*, 178–182.
- [28] N. A. Manan, C. Hardacre, J. Jacquemin, D. W. Rooney, T. G. A. Youngs, *J. Chem. Eng. Data* **2009**, *54*, 2005–2022.
- [29] J. Palomar, M. Gonzalez-Miquel, A. Polo, F. Rodriguez, *Ind. Eng. Chem. Res.* **2011**, *50*, 3452–3463.
- [30] K. Z. Sumon, A. Henni, *Fluid Phase Equilibria* **2011**, *310*, 39–55.
- [31] J. Abildskov, M. D. Ellegaard, J. P. O’Connell, *Fluid Phase Equilibria* **2009**, *286*, 95–106.
- [32] J. S. Andreu, L. F. Vega, *J. Phys. Chem. B* **2008**, *112*, 15398–15406.
- [33] X. Zhang, Z. Liu, W. Wang, *AIChE* **2008**, *54*, 2717–2728.
- [34] J. S. Andreu, L. F. Vega, *J. Phys. Chem. C* **2007**, *111*, 16028–16034.
- [35] Y. S. Kim, J. H. Jang, B. D. Lim, J. W. Kang, C. S. Lee, *Fluid Phase Equilibria* **2007**, *256*, 70–74.
- [36] A. A. Oliferenko, P. Oliferenko, K. R. Seddon, J. S. Torrecilla, *Phys. Chem. Chem. Phys.* **2011**, *13*, 17262–17272.
- [37] E. J. Maginn, *J. Phys.: Condens. Matter* **2009**, *21*, 373101–37318.
- [38] W. Shi, E. J. Maginn, *J. Phys. Chem. B* **2008**, *112*, 2045–2055.
- [39] W. Shi, E. J. Maginn, *J. Phys. Chem. B* **2008**, *112*, 16710–16720.
- [40] T. K  ddermann, D. Paschek, R. Ludwig, *ChemPhysChem* **2008**, *9*, 549–555.
- [41] R. M. Lynden-Bell, N. A. Atamas, A. Vasilyuk, C. G. Hanke, *Mol. Phys.* **2002**, *100*, 3225–3229.
- [42] C. G. Hanke, A. Johansson, J. B. Harper, R. M. Lynden-Bell, *Chem. Phys. Lett.* **2003**, *374*, 85–89.
- [43] J. Deschamps, M. F. Costa Gomes, A. A. H. Padua, *ChemPhysChem* **2004**, *5*, 1049–1052.
- [44] J. K. Shah, E. J. Maginn, *Fluid Phase Equilibria* **2004**, *195*, 222–223.
- [45] J. K. Shah, E. J. Maginn, *J. Phys. Chem. B* **2005**, *109*, 10395–10405.
- [46] C. Cadena, J. L. Anthony, J. K. Shah, T. I. Morrow, J. F. Brennecke, E. J. Maginn, *J. Am. Chem. Soc.* **2004**, *126*, 5300–5308.
- [47] J. Kumelan, A. P. S. Kamps, I. Urukova, D. Tuma, G. Maurer, *J. Chem. Thermodynamics* **2005**, *37*, 595–602.
- [48] I. Urukova, J. Vorholz, G. Maurer, *J. Phys. Chem. B* **2005**, *109*, 12154–12159.
- [49] J. Kumelan, A. P. S. Kamps, D. Tuma, G. Maurer, *Ind. Eng. Chem. Res.* **2007**, *46*, 8236–8240.
- [50] J. Deschamps, , A. A. H. P  dua, *ACS Symp. Series* **2005**, *901*, 150–158.
- [51] X. P. Wu, Z. P. Liu, W. C. Wang, *Wuli Huaxue Xuebao* **2005**, *21*, 1138–1142.
- [52] W. Shi, D. C. Sorescu, D. R. Luebke, M. J. Keller, S. Wickramanayake, *J. Phys. Chem. B* **2010**, *114*, 6531–6541.
- [53] A. F. Ghobadi, V. Taghikhani, J. R. Elliott, *J. Phys. Chem. B* **2011**, *115*, 13599–13607.
- [54] F. Dommert, K. Wendler, R. Berger, L. Delle Site, C. Holm, *ChemPhysChem* **2012**, *13*, 1625–1637.
- [55] J. N. Canongia Lopes, J. Deschamps, A. A. H. Padua, *J. Phys. Chem. B* **2004**, *108*, 2038–2047.
- [56] T. K  ddermann, D. Paschek, R. Ludwig, *ChemPhysChem* **2007**, *8*, 2464–2470.
- [57] D. Paschek, T. K  ddermann, R. Ludwig, *Phys. Rev. Lett.* **2008**, *100*, 115901.
- [58] D. Kerl  , R. Ludwig, A. Geiger, D. Paschek, *J. Phys. Chem. B* **2009**, *113*, 12727–12735.
- [59] L. R. Pratt, *Annu. Rev. Phys. Chem.* **2003**, *53*, 409–436.
- [60] N. T. Southall, K. A. Dill, A. D. J. Haymet, *J. Phys. Chem. B* **2002**, *106*, 521–533.
- [61] B. Widom, P. Bhimalapuram, K. Koga, *Phys. Chem. Chem. Phys.* **2003**, *5*, 3085–3093.
- [62] D. Chandler, *Nature (London)* **2005**, *437*, 640–647.
- [63] B. Wittich, U. K. Deiters, *J. Phys. Chem. B* **2010**, *114*, 3452–3463.
- [64] K. Patkowski, W. Cencek, P. Jankowski, K. Szalewicz, J. Mehl, G. Garberoglio, A. H. Harvey, *J. Chem. Phys.* **2008**, *129*, 094304–094323.
- [65] B. Guillot, Y. Guissani, *J. Chem. Phys.* **1993**, *99*, 8075–

- 8094.
- [66] J. Potoff, J. I. Siepmann, *AIChE Journal* **2001**, *47*, 1676–1682.
- [67] N. Hansen, F. A. B. Agbor, F. J. Keil, *Fluid Phase Equilibria* **2007**, *259*, 180–188.
- [68] J. G. Harris, K. H. Yung, *J. Phys. Chem.* **1995**, *99*, 12021–12024.
- [69] E. Lindahl, B. Hess, D. van der Spoel, *J. Mol. Model.* **2001**, *7*, 306–317.
- [70] D. Paschek, MOSCITO 4: MD simulation package, **2008**, <http://ganter.chemie.uni-dortmund.de/MOSCITO>.
- [71] S. Nosé, *Mol. Phys.* **1984**, *52*, 255–268.
- [72] W. G. Hoover, *Phys. Rev. A* **1985**, *31*, 1695–1697.
- [73] M. Parrinello, A. Rahman, *J. Appl. Phys.* **1981**, *52*, 7182–7180.
- [74] S. Nosé, M. L. Klein, *Mol. Phys.* **1983**, *50*, 1055–1076.
- [75] U. Essmann, L. Perera, M. L. Berkowitz, T. A. Darden, H. Lee, L. G. Pedersen, *J. Chem. Phys.* **1995**, *103*, 8577–8593.
- [76] J. P. Ryckaert, G. Ciccotti, H. J. C. Berendsen, *J. Comp. Phys.* **1977**, *23*, 327–341.
- [77] R. P. Kennan, G. L. Pollack, *J. Chem. Phys.* **1990**, *93*, 2724–2735.
- [78] B. Widom, *J. Chem. Phys.* **1963**, *39*, 2808–2812.
- [79] T. L. Beck, M. E. Paulaitis, L. R. Pratt, *The Potential Distribution Theorem and Models of Molecular Solutions*, Cambridge University Press, Cambridge, UK, **2006**.
- [80] C. H. Bennett, *J. Comp. Phys.* **1976**, *22*, 245–268.
- [81] K. S. Shing, K. E. Gubbins, *Mol. Phys.* **1983**, *49*, 1121–1138.
- [82] D. Frenkel, B. Smit, *Understanding Molecular Simulation. From Algorithms to Applications*, 2nd Aufl., Academic Press, San Diego, **2002**.
- [83] D. Paschek, *J. Chem. Phys.* **2004**, *120*, 6674–6690.
- [84] J. E. Roberts, J. Schnitker, *J. Chem. Phys.* **1994**, *101*, 5024–5031.
- [85] D. Paschek, *J. Chem. Phys.* **2004**, *120*, 10605–10617.
- [86] To interconvert solvation free energies μ_{ex} and Henry constants k_{H} , we use a second order polynomial fitted to the temperature dependent ion-pair density of the simulated ionic liquids: $\rho_{\text{IL}}(T) = \rho_{\text{IL}}^{(0)} + \rho_{\text{IL}}^{(1)} \cdot T + \rho_{\text{IL}}^{(2)} \cdot T^2$.
 [C₂mim][NTf₂]: $\rho_{\text{IL}}^{(0)} = 2.985 \text{ nm}^{-3}$, $\rho_{\text{IL}}^{(1)} = -2.51 \times 10^{-3} \text{ nm}^{-3} \text{ K}^{-1}$, and $\rho_{\text{IL}}^{(2)} = 8.46 \times 10^{-7} \text{ nm}^{-3} \text{ K}^{-2}$.
 [C₄mim][NTf₂]: $\rho_{\text{IL}}^{(0)} = 2.639 \text{ nm}^{-3}$, $\rho_{\text{IL}}^{(1)} = -2.18 \times 10^{-3} \text{ nm}^{-3} \text{ K}^{-1}$, and $\rho_{\text{IL}}^{(2)} = 6.85 \times 10^{-7} \text{ nm}^{-3} \text{ K}^{-2}$.
 [C₆mim][NTf₂]: $\rho_{\text{IL}}^{(0)} = 2.368 \text{ nm}^{-3}$, $\rho_{\text{IL}}^{(1)} = -1.94 \times 10^{-3} \text{ nm}^{-3} \text{ K}^{-1}$, and $\rho_{\text{IL}}^{(2)} = 5.90 \times 10^{-7} \text{ nm}^{-3} \text{ K}^{-2}$.
 [C₈mim][NTf₂]: $\rho_{\text{IL}}^{(0)} = 2.127 \text{ nm}^{-3}$, $\rho_{\text{IL}}^{(1)} = -1.56 \times 10^{-3} \text{ nm}^{-3} \text{ K}^{-1}$, and $\rho_{\text{IL}}^{(2)} = 2.92 \times 10^{-7} \text{ nm}^{-3} \text{ K}^{-2}$.
- [87] K. N. Marsh, J. F. Brennecke, R. D. Chirico, M. Frenkel, A. Heintz, J. W. Magee, C. J. Peters, L. P. N. Rebelo, K. R. Seddon, *Pure Appl. Chem.* **2009**, *81*, 781–790.
- [88] R. D. Chirico, V. Diky, J. W. Magee, M. Frenkel, K. N. Marsh, *Pure Appl. Chem.* **2009**, *81*, 791–828.
- [89] J. Kumelan, A. P. S. Kamps, D. Tuma, G. Maurer, *J. Chem. Thermodynamics* **2006**, *38*, 1396–1401.
- [90] S. S. Moganty, R. E. Baltus, *Ind. Eng. Chem. Res.* **2010**, *49*, 5846–5853.
- [91] D. Kerlé, R. Ludwig, A. Geiger, D. Paschek, *Z. Phys. Chem.* **2013**, *227*, 167–176.
- [92] D. Camper, J. Bara, C. Koval, R. Noble, *Ind. Eng. Chem. Res.* **2006**, *45*, 6279–6283.
- [93] J. L. Anderson, J. K. Dixon, J. F. Brennecke, *Acc. Chem. Res.* **2007**, *40*, 1208–1216.
- [94] J. Blath, M. Christ, N. Deubler, T. Hirth, T. Schiestel, *Chem. Eng. J.* **2011**, *172*, 167–176.
- [95] W. Afzal, X. Liu, J. M. Prausnitz, *J. Chem. Thermodynamics* **2013**, *63*, 88–94.
- [96] J. Kumelan, A. P. S. Kamps, D. Tuma, G. Maurer, *J. Chem. Eng. Data* **2009**, *54*, 966–971.
- [97] J. L. Anthony, J. L. Anderson, E. J. Maginn, J. F. Brennecke, *J. Phys. Chem. B* **2005**, *109*, 6366–6374.
- [98] J. Kumelan, A. P. S. Kamps, D. Tuma, G. Maurer, *J. Chem. Eng. Data* **2006**, *51*, 1364–1367.
- [99] R. Simha, T. Somcynsky, *Macromolecules* **1969**, *2*, 342–350.
- [100] H. Xie, R. Simha, *Polymer Int.* **1997**, *44*, 348–355.
- [101] J. N. Onuchic, Z. Luthey-Schulten, P. G. Wolynes, *Annu. Rev. Phys. Chem.* **1997**, *48*, 545–600.
- [102] W. Hayduk, H. Laudie, *AIChE Journal* **1973**, *19*, 1233–1238.
- [103] D. Beutier, H. Renon, *AIChE Journal* **1978**, *24*, 1122–1125.
- [104] L. P. N. Rebelo, J. N. Canongia Lopes, J. M. S. S. Esperança, E. Filipe, *J. Phys. Chem B* **2005**, *109*, 6040–6043.
- [105] M. G. Freire, P. J. Carvalho, A. M. Fernandes, I. M. Marrucho, A. J. Queimada, J. A. P. Coutinho, *J. Colloid Interf. Sci.* **2007**, *314*, 621–630.
- [106] A. Yokozeki, M. B. Shiflett, C. P. Junk, L. M. Grieco, T. Foo, *J. Phys. Chem. B* **2008**, *112*, 16654–16663.
- [107] E.-K. Shin, B.-C. Lee, J. S. Lim, *J. Supercrit. Fluids.* **2008**, *45*, 282–292.
- [108] J. O. Valderrama, P. A. Robles, *Ind. Eng. Chem. Res.* **2007**, *46*, 1338–1344.